

Empowering Image Recovery: A Multi-Attention Approach

Juan Wen^{1,2} Yawei Li² Chao Zhang³ Weiyan Hou¹ Radu Timofte^{2,4} Luc Van Gool²

¹ Zhengzhou University ² Computer Vision Lab, ETH Zurich

³ LAN-XEN, Technology, INC. ⁴ Bayerische Julius-Maximilians-Universität Würzburg

Abstract

We propose *Diverse Restormer (DART)*, a novel image restoration method that effectively integrates information from various sources (long sequences, local and global regions, feature dimensions, and positional dimensions) to address restoration challenges. While Transformer models have demonstrated excellent performance in image restoration due to their self-attention mechanism, they face limitations in complex scenarios. Leveraging recent advancements in Transformers and various attention mechanisms, our method utilizes customized attention mechanisms to enhance overall performance. *DART*, our novel network architecture, employs windowed attention to mimic the selective focusing mechanism of human eyes. By dynamically adjusting receptive fields, it optimally captures the fundamental features crucial for image resolution reconstruction. Efficiency and performance balance are achieved through the *LongIR* attention mechanism for long sequence image restoration. Integration of attention mechanisms across feature and positional dimensions further enhances the recovery of fine details. Evaluation across five restoration tasks consistently positions *DART* at the forefront. Upon acceptance, we commit to providing publicly accessible code and models to ensure reproducibility and facilitate further research.

1. Introduction

Image restoration constitutes a foundational area of research within computer vision and image processing, exerting a pivotal influence across diverse applications. Its primary objective is to enhance image quality, thereby facilitating a more precise and vivid representation of objects and scenes, ultimately enriching visual perception. Specifically, it encompasses the process of improving or recovering the quality and visual fidelity of digital images that have undergone degradation or damage due to factors such as noise, blur, or other forms of distortion.

Transformers have garnered widespread acclaim for their effectiveness in bolstering visual perception and enhancing

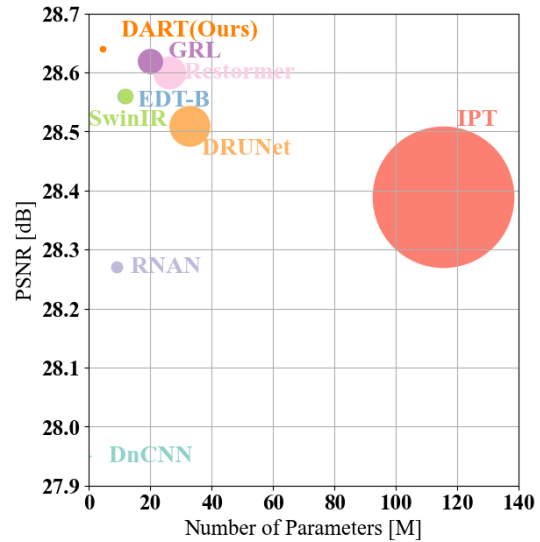


Figure 1. (Color image Denoising CBS68 dataset) (Noise level: 50) Our *DART-B* network performs denoising tasks with just 4.5M parameters, achieving the state-of-the-art level for this task. Prior works such as *GRL-B* [35] utilized 19.81M parameters, *Restormer* [68] used 26.13M parameters, and *SwinIR* [36] employed 11.75M parameters.

the performance of various computer vision tasks, including image restoration [36, 38]. Spearheaded by Vaswani *et al.* [61] Liang *et al.* [36] and Li *et al.* [35], underscore the remarkable capabilities of Transformers in tackling challenges associated with image restoration, encompassing tasks like noise reduction and blur correction.

While Transformer models excel in capturing complex relationships within data through their self-attention mechanism, they may face challenges in achieving significant gains in certain intricate image restoration tasks. For instance, *Restormer* has demonstrated substantial improvements across multiple image restoration tasks [68]. Introducing a Channel-based self-attention mechanism, *Restormer* effectively addresses specific challenges in image restoration tasks. However, its complexity increases with the number of channels, rendering it impractical for high-resolution image restoration tasks.

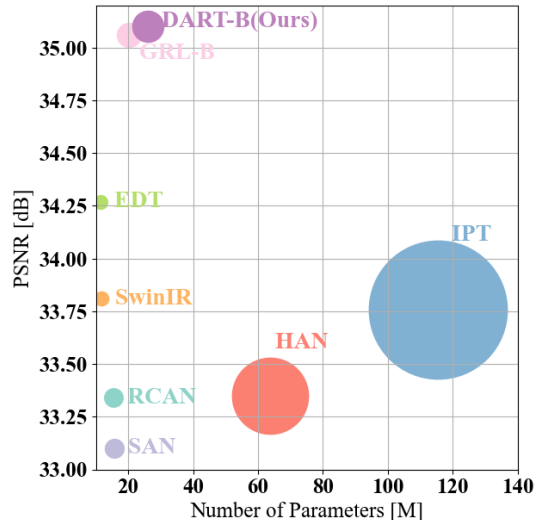


Figure 2. Image SR×2 on Urban100 dataset.

To address the limitations of existing models, we propose a novel multi-attention transformer for image restoration—Diverse Attention Fusion Restoration Transformer (DART), illustrated in Figure 3. DART incorporates several key designs within its attention mechanism module, enabling the model to focus on various aspects of complex patterns and enhance its ability to recover fine details. Extensive experiments unequivocally demonstrate the effectiveness of our proposed Diverse Restormer model, showcasing its prowess in handling complex image restoration tasks.

We utilize the SwinIR network as the infrastructure for our model [36]. An essential module in our Diverse Attention Fusion Restoration Transformer (DART) model is the Long Sequence Image Restoration (LongIR) module (refer to Figure 3, DART(C)). To address the limitations of SwinIR in handling long sequences due to the quadratic scaling of self-attention operations with sequence length, we propose the LongIR approach. This module employs an attention mechanism that linearly scales with sequence length, enabling it to effortlessly handle thousands of tokens or even longer sequences. We compute the attention for LongIR using X_w (where X_d denotes the input). Subsequently, we combine the window attention of multiple heads with LongIR attention and pass the result to fully connected layers to obtain the merged X . Finally, we apply another crucial module in our DART model called feature dimension attention and position dimension attention (refer to Figure 4) to perform additional attention computations on the merged data X , yielding the Refined Feature X .

The integration of the Long Sequence Image Restoration module facilitates the effective management of sequences through the combination of global and local attention mechanisms. Feature dimension and position dimension attention mechanisms assist neural networks in focusing on specific information within feature maps. Feature dimension attention enhances the representation and utilization of dif-

ferent feature dimensions (feature maps) within the feature map by emphasizing or de-emphasizing certain feature dimensions to improve the network’s performance on specific tasks. Conversely, position dimension attention selectively focuses on specific spatial dimensions within images or feature maps, allowing the model to emphasize or de-emphasize certain parts of the input data, thereby enhancing its ability to capture relevant information and improve task performance. This design approach leverages LongIR Attention, Position Dimension Attention, and Feature Dimension Attention, enabling the model to extract information from long sequences, local and global contexts, as well as specific feature dimensions and different Positional Dimension dimensions.

In summary, our paper presents three key contributions:

Novel Multi-Attention Transformer: We propose Collaborative Image Restoration with Integrated Attention Mechanisms, a novel multi-attention transformer (DART). DART integrates LongIR along with Position Dimension Attention and Feature Dimension Attention mechanisms, enhancing the model’s ability to recover fine details from various complex patterns.

Efficient Experimental Design: To strike a balance between performance and efficiency, we propose an effective experimental design. Our collaborative image restoration model, incorporating multi-attention mechanisms, reduces computational load by decreasing the number of model layers without a significant impact on performance.

State-of-the-Art Results: Our approach achieves state-of-the-art results in image super-resolution, denoising, motion deblurring, and defocus deblurring. Notably, our DART-B network outperforms previous works with only 4.5M parameters, showcasing superiority over GRL-B [35] (19.81M parameters), Restormer [68] (26.13M parameters), and SwinIR [36] (11.75M parameters) in denoising tasks.

2. Related Works

2.1. Image Restoration

In recent years, data-driven CNN architectures [6, 14, 64, 66, 75, 77] have consistently outperformed traditional restoration methods [20, 27, 41, 57]. Among convolutional designs, U-Net architectures [3, 12, 29, 62, 64, 67, 73] have been extensively studied for restoration, thanks to their hierarchical multi-scale representation and computational efficiency. Similarly, skip connection-based approaches have proven effective for restoration, focusing on learning residual signals [18, 37, 66, 76]. Spatial and channel attention modules have been incorporated to selectively attend to relevant information [34, 64, 66]. For major design choices in image restoration, readers can refer to NTIRE challenge reports [2, 4, 22, 44] and recent literature reviews [7, 32, 56].

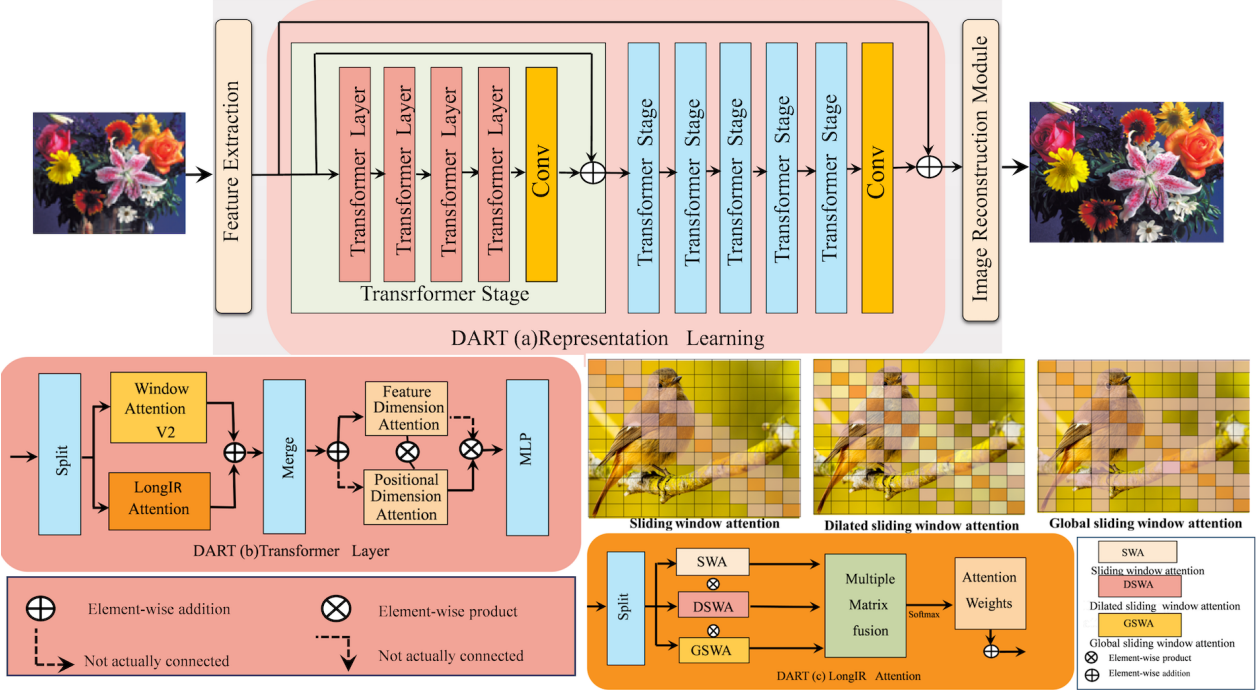


Figure 3. Network Architecture. (a) Illustrates the learning module comprising stages of transformer layers. (b) The Transformer module utilizes LongIR (Sliding Window Attention, Expanded Sliding Window Attention, Global Attention) along with Position Dimension Attention and Feature Dimension Attention mechanisms to extract information from long sequences, local, global, specific feature dimensions, and different Positional Dimension dimensions regions for image restoration. (c) Demonstrates the working mechanism of LongIR Attention.

2.2. Vision Transformer

The Restormer image restoration model proposed by Zamir *et al.* exhibits increased computational complexity with the growing number of channels, making it impractical for high-resolution image restoration tasks [68]. Inspired by the success of pre-training transformer-based models in natural language processing (NLP), researchers introduced a transformer model designed for image restoration in 2021. This model, known as the Image Processing Transformer (IPT) [11], is noteworthy. However, IPT employs an extensive parameter count (exceeding 115.5M), utilizes large-scale datasets (over 1.1M images), and incorporates multi-task learning for optimal performance. In this paper, we introduce the Diverse Restormer (DART) approach, which employs model integration to effectively extract information from long sequences, local and global contexts, specific feature dimensions, and various positional dimension regions. The model aims to strike a balance between efficiency and performance, leveraging multiple attention mechanisms to focus on different aspects of complex patterns, thereby enhancing its ability to recover fine details [36, 38, 68].

3. Method

In this section, we address the primary research question: Why is collectively extracting information from long sequences, local and global contexts, specific feature di-

mensions, and various positional dimension regions crucial for image restoration?

3.1. Motivation

The Swin Transformer [38] has demonstrated excellent performance in image super-resolution. Therefore, we have chosen SwinIR [36] as the framework for our entire network architecture. We observed that the SwinIR [36] model based on the Transformer is unable to handle long sequences due to its self-attention operations, which scale quadratically with sequence length. To address this limitation, we introduced the LongIR (See Figure 3(c)) with an attention mechanism that linearly extends with the sequence length, allowing it to easily handle thousands of tokens or longer information. It can also combine local window attention with task-driven global attention. Furthermore, the transformer model replaces attention matrices with sparse matrices to improve speed.

We reviewed the literature on image restoration over the past three years and found that the Restormer model proposed by Zamir *et al.* [68] has performed well in the field. However, its computational complexity grows quadratically with the number of channels, making it impractical for high-resolution image restoration tasks. To address this issue, we adopt feature dimension attention and position dimension attention to assist neural networks in focusing on information within feature maps. Feature dimension attention

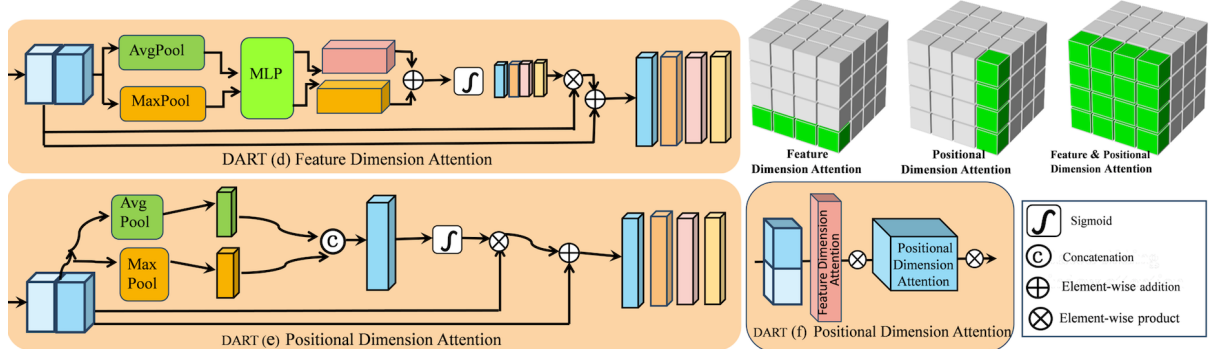


Figure 4. (d), (e), and (f) illustrate the working mechanisms of Position Dimension Attention and Feature Dimension Attention.

emphasizes or attenuates specific features to enhance the network’s performance on particular tasks. Position dimension attention selectively attends to specific spatial regions within images or feature maps, allowing the model to highlight or downplay certain parts of the input data, thereby enhancing its ability to capture relevant information and improve task performance.

Chen *et al.* proposed a transformer model for image restoration called Image Processing Transformer (IPT) [11]. However, IPT relies on a large number of parameters (exceeding 115.5M parameters), large-scale datasets (over 1.1M images), and multi-task learning for good performance. In order to design a complementary attention mechanism to address different problems in the task, we propose the Diverse Restorer (DART) image restoration model.

3.2. Network architecture

Our network architecture, illustrated in Figure 3(a), comprises three main modules: shallow feature extraction, deep feature extraction, and high-quality image reconstruction. The first and last modules rely on CNN, while the intermediate module utilizes SwinTransformer [38] (refer to Figure 3(b)). Transformer’s deep feature extraction module combines LongIR with (sliding-window attention, expanding sliding-window attention, global attention) and feature dimension attention mechanism, position dimension attention mechanism.

The crucial layer extracts region-specific details from long sequences, local, global contexts, as well as feature dimension and position dimension attention mechanisms. Initially, it utilizes the window attention module from SwinTransformer V2 to process information [38] and compute the long attention module. Subsequently, it integrates information from multiple multi-head attentions and LongIR (refer to Figure 3(c)), passing it to the fully connected layer for feature fusion. Finally, attention computations are performed using position dimension and feature dimension attention mechanisms (see Figure 4(d, e, f) to obtain processed data from five attention modules.

The core mechanism of LongIR [8] uses three attention windows.

Sliding window attention (Extract local information)

This attention mechanism can be compared to a convolution kernel, and the size of each convolution kernel is our receptive field. The essence is to set a fixed size window w , which stipulates that each Token in the sequence can only be seen for W adjacent Tokens, $W - \frac{1}{2}$ Tokens can be seen on each side of the left and right sides. In this way, the time complexity changes from the original $O(N \times N)$ to $O(N \times W)$, where $W < N$. Moreover, we don’t need to worry that this setting cannot establish the information of the entire sequence, because the transformer model structure itself is a layer-by-layer structure. The high-level model has a wider receptive field than the bottom layer, so more information can be seen. so it has the ability to model a global representation that integrates all sequence information. Through this setting, LongIR can achieve a better balance between modeling quality and efficiency.

Expanding sliding window attention (Extract long sequence information)

This attention window is set to make up for the lack of length caused by the previous window. A gap of size d is set between the two Tokens without increasing the time complexity. Then the range of the receptive field can be extended to $d \times w$.

Global attention (Extract global information)

The whole world here is only part of the whole world. Here we only set certain specific tokens to be able to see all other tokens. For other tokens that are not too important, we still use sliding window attention. Therefore, its attention includes self-attention of windowed local contextual information and global attention activated by terminal tasks. Local attention is used to establish local contextual information representation, and global attention is used to establish a complete sequence representation for prediction. As mentioned earlier, the time and space complexity of existing attention calculation methods are $O(n^2)$, which makes it difficult to train on long sequences. Therefore, the model uses (attention pattern) to sparse the complete self-attention matrix, which perfectly solves this problem.

Feature Dimension Attention Module

The Feature Di-

Table 1. *Color and grayscale image denoising* results. Model complexity and prediction accuracy are shown for better comparison.

Method	# Params [M]	Color									Grayscale											
		CBSD68 [39]			Kodak24 [15]			McMaster [74]			Urban100 [21]			Set12 [71]			BSD68 [39]			Urban100 [21]		
		$\sigma=15$	$\sigma=25$	$\sigma=50$	$\sigma=15$	$\sigma=25$	$\sigma=50$	$\sigma=15$	$\sigma=25$	$\sigma=50$	$\sigma=15$	$\sigma=25$	$\sigma=50$	$\sigma=15$	$\sigma=25$	$\sigma=50$	$\sigma=15$	$\sigma=25$	$\sigma=50$	$\sigma=15$	$\sigma=25$	$\sigma=50$
DnCNN [24]	0.56	33.90	31.24	27.95	34.60	32.14	28.95	33.45	31.52	28.62	32.98	30.81	27.59	32.86	30.44	27.18	31.73	29.23	26.23	32.64	29.95	26.26
RNAN [76]	8.96	-	-	28.27	-	-	29.58	-	-	29.72	-	-	29.08	-	-	27.70	-	-	26.48	-	-	27.65
IPT [11]	115.33	-	-	28.39	-	-	29.64	-	-	29.98	-	-	29.71	-	-	-	-	-	-	-	-	-
EDT-B [33]	11.48	34.39	31.76	28.56	35.37	32.94	29.87	35.61	33.34	30.25	35.22	33.07	30.16	-	-	-	-	-	-	-	-	-
DRUNet [73]	32.64	34.30	31.69	28.51	35.31	32.89	29.86	35.40	33.14	30.08	34.81	32.60	29.61	33.25	30.94	27.90	31.91	29.48	26.59	33.44	31.11	27.96
SwinIR [36]	11.75	34.42	31.78	28.56	35.34	32.89	29.79	35.61	33.20	30.22	35.13	32.90	29.82	33.36	31.01	27.91	31.97	29.50	26.58	33.70	31.30	27.98
Restormer [68]	26.13	34.40	31.79	28.60	35.47	33.04	30.01	35.61	33.34	30.30	35.13	32.96	30.02	33.42	31.08	28.00	31.96	29.52	26.62	33.79	31.46	28.29
GRL-B [35]	19.81	34.45	31.82	28.62	35.43	33.02	29.93	35.73	33.46	30.36	35.54	33.35	30.46	33.47	31.12	28.03	32.00	29.54	26.60	34.09	31.80	28.59
DART-B(ours)	4.5	34.49	31.85	28.64	35.49	33.06	30.05	35.79	33.52	30.39	35.56	33.39	30.50	33.50	31.15	28.03	32.00	29.56	26.63	34.11	31.82	28.61

mension attention is computed as:

$$\begin{aligned} \mathbf{M}_c(\mathbf{F}) &= \sigma(MLP(AvgPool(\mathbf{F})) + MLP(MaxPool(\mathbf{F}))) \\ &= \sigma(\mathbf{W}_1(\mathbf{W}_0(\mathbf{F}_{avg}^c)) + \mathbf{W}_1(\mathbf{W}_0(\mathbf{F}_{max}^c))), \end{aligned} \quad (1)$$

where σ denotes the sigmoid function, $\mathbf{W}_0 \in \mathbb{R}^{C/r \times C}$, and $\mathbf{W}_1 \in \mathbb{R}^{C \times C/r}$. Note that the MLP weights, \mathbf{W}_0 and \mathbf{W}_1 , are shared for both inputs and the ReLU activation function is followed by \mathbf{W}_0 .

The input feature map F with dimensions $H \times W \times C$ undergoes global max pooling and global average pooling along the width and height, resulting in two $1 \times 1 \times C$ features. These features are then fed into a shared two-layer neural network (MLP). The first layer has C/r neurons (with r as the reduction rate) and uses the ReLU activation function, while the second layer has C neurons. The output from the MLP undergoes element-wise summation and sigmoid activation, generating the final Feature Dimension attention feature denoted as M_c . Finally, the Feature Dimension attention feature M_c undergoes an element-wise multiplication with the input feature map F , producing the input features required for the Positional Dimension attention module.

Positional Dimension Attention Module The Positional Dimension attention is computed as:

$$\begin{aligned} \mathbf{M}_s(\mathbf{F}) &= \sigma(f^{7 \times 7}([AvgPool(\mathbf{F}); MaxPool(\mathbf{F})])) \\ &= \sigma(f^{7 \times 7}([\mathbf{F}_{avg}^s; \mathbf{F}_{max}^s])), \end{aligned} \quad (2)$$

where σ denotes the sigmoid function and $f^{7 \times 7}$ represents a convolution operation with the filter size of 7×7 .

The feature map F output by the Feature Dimension attention module is used as the input feature map of this module. First, do a Feature Dimension-based global max pooling and global average pooling to obtain two $H \times W \times 1$ feature maps, and then perform a concat operation (Feature Dimension splicing) on these two feature maps based on the Feature Dimension. Then, after a 7×7 convolution operation (7×7 is better than 3×3), the dimension is reduced to 1 Feature Dimension, that is, $H \times W \times 1$. Then the Positional Dimension attention feature, namely M_s , is generated through sigmoid. Finally, the feature is multiplied by

the input feature of the module to obtain the final generated feature .

4. Experiments

4.1. Experimental Setup

We assess the performance of our Diverse Restormer (DART) image restoration model across a spectrum of tasks, encompassing:

- 1) Real Image Restoration:**
 - Motion Deblurring:** We evaluate our approach on the GoPro and HIDE datasets, comparing against 15 state-of-the-art methods.
 - Defocus Deblurring:** Comparative evaluations are conducted on outdoor, indoor, and combined scene datasets, against 14 state-of-the-art methods.
 - Real Image Denoising:** We assess performance against 13 state-of-the-art methods using the SIDD and DND datasets.
- 2) Synthetic Data-Based Restoration:**
 - Denoising:** Evaluation is performed on color (CBSD68, Kodak24, McMaster, Urban100) and grayscale (Set12, BSD68, Urban100) images from multiple datasets, compared against 8 state-of-the-art methods.
 - Single Image Super-Resolution (SR):** We examine performance using classical datasets (Set5, Set14, BSD100, Urban100, Manga109) for 2x, 3x, and 4x upscaling comparisons, against 7 advanced methods.

We present two model sizes, namely DART-S and DART-B, offering a comprehensive perspective on image restoration ranging from global to local considerations. Additional details on the models, datasets, and results are provided in the supplementary material. The network is trained using the Adam optimizer and L1 loss, with an initial learning rate of 2×10^{-4} for both real and synthetic image restoration tasks.

4.2. Experimental Results

In this section, we address the second research question by examining the performance of our proposed network across various images. ‘‘How does the performance of collaborative image restoration with integrated attention mechanisms compare?’’

Table 2. *Classical image SR* results. Results of lightweight models and accurate models are summarized.

Method	Scale	# Params [M]	Set5 [9]		Set14 [69]		BSD100 [39]		Urban100 [21]		Manga109 [40]	
			PSNR↑	SSIM↑	PSNR↑	SSIM↑	PSNR↑	SSIM↑	PSNR↑	SSIM↑	PSNR↑	SSIM↑
RCAN [75]	x2	15.44	38.27	0.9614	34.12	0.9216	32.41	0.9027	33.34	0.9384	39.44	0.9786
SAN [13]	x2	15.71	38.31	0.9620	34.07	0.9213	32.42	0.9028	33.10	0.9370	39.32	0.9792
HAN [45]	x2	63.61	38.27	0.9614	34.16	0.9217	32.41	0.9027	33.35	0.9385	39.46	0.9785
IPT [11]	x2	115.48	38.37	-	34.43	-	32.48	-	33.76	-	-	-
SwinIR [36]	x2	0.88	38.14	0.9611	33.86	0.9206	32.31	0.9012	32.76	0.9340	39.12	0.9783
SwinIR [36]	x2	11.75	38.42	0.9623	34.46	0.9250	32.53	0.9041	33.81	0.9427	39.92	0.9797
EDT [33]	x2	0.92	38.23	0.9615	33.99	0.9209	32.37	0.9021	32.98	0.9362	39.45	0.9789
EDT [33]	x2	11.48	38.63	0.9632	34.80	0.9273	32.62	0.9052	34.27	0.9456	40.37	0.9811
GRL-S [35]	x2	3.34	38.37	0.9632	34.64	0.9280	32.52	0.9069	34.36	0.9463	39.84	0.9793
GRL-B [35]	x2	20.05	38.67	0.9647	35.08	0.9303	32.67	0.9087	35.06	0.9505	40.67	0.9818
DART-S(ours)	x2	4.70	38.38	0.9632	34.66	0.9281	32.55	0.9071	34.38	0.9464	39.86	0.9795
DART-B(ours)	x2	25.99	38.69	0.9648	35.11	0.9304	32.72	0.9089	35.10	0.9507	40.71	0.9820
RCAN [75]	x3	15.44	34.74	0.9299	30.65	0.8482	29.32	0.8111	29.09	0.8702	34.44	0.9499
SAN [13]	x3	15.71	34.75	0.9300	30.59	0.8476	29.33	0.8112	28.93	0.8671	34.30	0.9494
HAN [45]	x3	63.61	34.75	0.9299	30.67	0.8483	29.32	0.8110	29.10	0.8705	34.48	0.9500
IPT [11]	x3	-	34.81	-	30.85	-	29.38	-	29.49	-	-	-
SwinIR [36]	x3	-	34.62	0.9289	30.54	0.8463	29.20	0.8082	28.66	0.8624	33.98	0.9478
SwinIR [36]	x3	0.9	34.97	0.9318	30.93	0.8534	29.46	0.8145	29.75	0.8826	35.12	0.9537
EDT [33]	x3	11.48	34.97	0.9316	30.89	0.8527	29.44	0.8142	29.72	0.8814	35.13	0.9534
DART-S(ours)	x3	3.99	34.76	0.9305	30.91	0.8535	29.21	0.8085	29.88	0.8823	35.15	0.9538
DART-B(ours)	x3	20.85	35.10	0.9328	31.05	0.8555	29.55	0.8163	30.22	0.8888	35.46	0.9551
RCAN [75]	x4	15.59	32.63	0.9002	28.87	0.7889	27.77	0.7436	26.82	0.8087	31.22	0.9173
SAN [13]	x4	15.86	32.64	0.9003	28.92	0.7888	27.78	0.7436	26.79	0.8068	31.18	0.9169
HAN [45]	x4	64.20	32.64	0.9002	28.90	0.7890	27.80	0.7442	26.85	0.8094	31.42	0.9177
IPT [11]	x4	115.63	32.64	-	29.01	-	27.82	-	27.26	-	-	-
SwinIR [36]	x4	0.90	32.44	0.8976	28.77	0.7858	27.69	0.7406	26.47	0.7980	30.92	0.9151
SwinIR [36]	x4	11.90	32.92	0.9044	29.09	0.7950	27.92	0.7489	27.45	0.8254	32.03	0.9260
EDT [33]	x4	0.92	32.53	0.8991	28.88	0.7882	27.76	0.7433	26.71	0.8051	31.35	0.9180
EDT [33]	x4	11.63	33.06	0.9055	29.23	0.7971	27.99	0.7510	27.75	0.8317	32.39	0.9283
GRL-S [35]	x4	3.49	32.76	0.9058	29.10	0.8007	27.90	0.7568	27.90	0.8357	32.11	0.9267
GRL-B [35]	x4	20.20	33.10	0.9094	29.37	0.8058	28.01	0.7611	28.53	0.8504	32.77	0.9325
DART-S(ours)	x4	3.96	32.80	0.9060	29.14	0.8008	27.96	0.7571	27.95	0.8443	32.13	0.9268
DART-B(ours)	x4	20.81	33.12	0.9095	29.39	0.8059	28.02	0.7610	28.55	0.8505	32.81	0.9326



Figure 5. The visual comparison of the DART-B network on x3SR utilizes red bounding boxes to highlight the patch for comparison, in order to better reflect performance differences.

We initially assessed the effectiveness of our proposed Diverse Restormer (DART) network in image restoration tasks using synthetic data. This included color and grayscale image denoising, classic image super-resolution (SR). Detailed complexities and accuracies are provided in Tables 1 and 2. 1) **Gaussian Denoising Task:** In this task, our network excels, particularly the DART-B baseline outperforming the state-of-the-art GRL-B method [35], despite having only one-fourth of GRL-B’s parameters. The more compact DART-S network approaches the performance of the previous state-of-the-art SwinIR [36] method,

showcasing the effectiveness of our approach compared to the GRL [35] method. This is particularly evident in focusing on global and local features, as well as long-range and Feature Dimension attention. Additionally, replacing the self-attention method with a long-range attention method in the SwinIR network proves effective in attention modeling. 2) **Classic Image Super-Resolution (SR):** Results for classic image SR are presented in Table 2, comparing the lightweight SR model with the classic SR model. Similar to Table 1, the conclusions are as follows: DART-S achieves a commendable balance between network complexity and SR

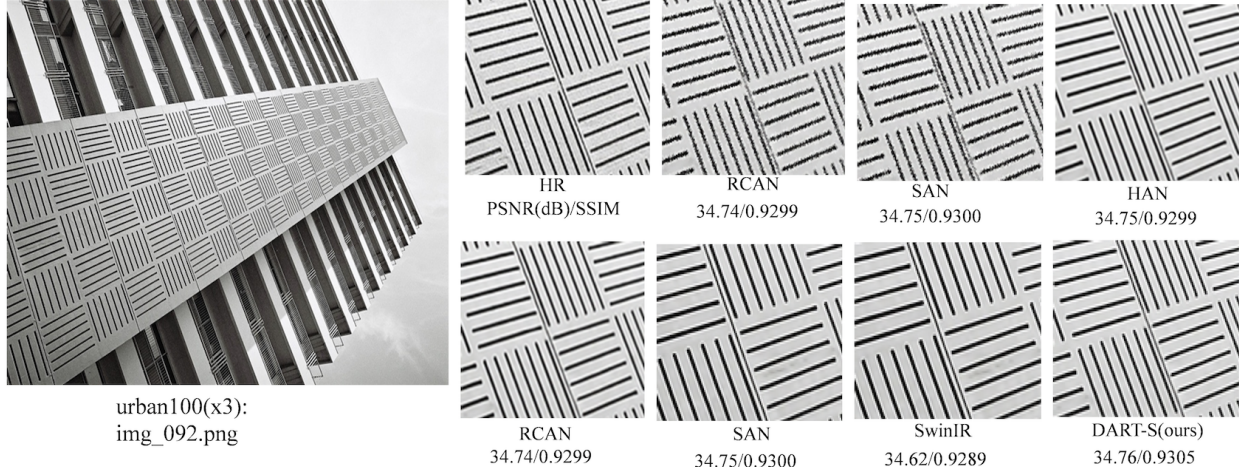


Figure 6. The visual comparison of the DART-S network on x3SR utilizes red bounding boxes to highlight the patch for comparison, in order to better reflect performance differences.

Table 3.

Defocus deblurring results. **S**: single-image defocus deblurring. **D**: dual-pixel defocus deblurring.

Method	Indoor Scenes				Outdoor Scenes				Combined			
	PSNR \uparrow	SSIM \uparrow	MAE \downarrow	LPIPS \downarrow	PSNR \uparrow	SSIM \uparrow	MAE \downarrow	LPIPS \downarrow	PSNR \uparrow	SSIM \uparrow	MAE \downarrow	LPIPS \downarrow
EBDB _S [23]	25.77	0.772	0.040	0.297	21.25	0.599	0.058	0.373	23.45	0.683	0.049	0.336
DMENet _S [30]	25.50	0.788	0.038	0.298	21.43	0.644	0.063	0.397	23.41	0.714	0.051	0.349
JNB _S [52]	26.73	0.828	0.031	0.273	21.10	0.608	0.064	0.355	23.84	0.715	0.048	0.315
DPDNet _S [3]	26.54	0.816	0.031	0.239	22.25	0.682	0.056	0.313	24.34	0.747	0.044	0.277
KPAC _S [53]	27.97	0.852	0.026	0.182	22.62	0.701	0.053	0.269	25.22	0.774	0.040	0.227
IFAN _S [31]	28.11	0.861	0.026	0.179	22.76	0.720	0.052	0.254	25.37	0.789	0.039	0.217
Restormer _S [68]	28.87	0.882	0.025	0.145	23.24	0.743	0.050	0.209	25.98	0.811	0.038	0.178
GRL _S -B [35]	29.06	0.886	0.024	0.139	23.45	0.761	0.049	0.196	26.18	0.822	0.037	0.168
DART _S -B(ours)	29.08	0.887	0.023	0.137	23.46	0.762	0.048	0.177	26.20	0.823	0.036	0.154
DPDNet _D [3]	27.48	0.849	0.029	0.189	22.90	0.726	0.052	0.255	25.13	0.786	0.041	0.223
RDPD _D [31]	28.10	0.843	0.027	0.210	22.82	0.704	0.053	0.298	25.39	0.772	0.040	0.255
Uformer _D [62]	28.23	0.860	0.026	0.199	23.10	0.728	0.051	0.285	25.65	0.795	0.039	0.243
IFAN _D [31]	28.66	0.868	0.025	0.172	23.46	0.743	0.049	0.240	25.99	0.804	0.037	0.207
Restormer _D [68]	29.48	0.895	0.023	0.134	23.97	0.773	0.047	0.175	26.66	0.833	0.035	0.155
GRL _D -B [35]	29.83	0.903	0.022	0.114	24.39	0.795	0.045	0.150	27.04	0.847	0.034	0.133
DART _D -B(ours)	29.85	0.904	0.021	0.112	24.41	0.796	0.043	0.140	27.06	0.848	0.033	0.121

Table 4. *Single-image motion deblurring* results. GoPro dataset [43] is used for training.

Method	GoPro [43]	HIDE [51]	Average
	PSNR \uparrow / SSIM \uparrow	PSNR \uparrow / SSIM \uparrow	PSNR \uparrow / SSIM \uparrow
DeblurGAN [28]	28.70 / 0.858	24.51 / 0.871	26.61 / 0.865
Nah <i>et al.</i> [43]	29.08 / 0.914	25.73 / 0.874	27.41 / 0.894
DeblurGAN-v2 [29]	29.55 / 0.934	26.61 / 0.875	28.08 / 0.905
SRN [55]	30.26 / 0.934	28.36 / 0.915	29.31 / 0.925
Gao <i>et al.</i> [16]	30.90 / 0.935	29.11 / 0.913	30.01 / 0.924
DBGAN [72]	31.10 / 0.942	28.94 / 0.915	30.02 / 0.929
MT-RNN [46]	31.15 / 0.945	29.15 / 0.918	30.15 / 0.932
DMPHN [70]	31.20 / 0.940	29.09 / 0.924	30.15 / 0.932
Suin <i>et al.</i> [54]	31.85 / 0.948	29.98 / 0.930	30.92 / 0.939
SPAIR [48]	32.06 / 0.953	30.29 / 0.931	31.18 / 0.942
MIMO-UNet+ [12]	32.45 / 0.957	29.99 / 0.930	31.22 / 0.944
IPT [11]	32.52 / -	- / -	- / -
MPRNet [67]	32.66 / 0.959	30.96 / 0.939	31.81 / 0.949
Restormer [68]	32.92 / 0.961	31.22 / 0.942	32.07 / 0.952
GRL-B [35]	33.93 / 0.968	31.65 / 0.947	32.79 / 0.958
DART-B (ours)	33.95 / 0.969	31.70 / 0.948	32.81 / 0.960

image quality in the lightweight network, while DART-B sets a new benchmark for precise image SR, reaching state-of-the-art levels.

We extended our network evaluation to real image restoration tasks, including 3) single-image defocus de-

Table 5. *Single-image motion deblurring* results on RealBlur [50] dataset. The networks are trained and tested on RealBlur dataset.

Method	RealBlur-R [50]	RealBlur-J [50]	Average
	PSNR \uparrow / SSIM \uparrow	PSNR \uparrow / SSIM \uparrow	PSNR \uparrow / SSIM \uparrow
DeblurGAN-v2 [29]	36.44 / 0.935	29.69 / 0.870	33.07 / 0.903
SRN [55]	38.65 / 0.965	31.38 / 0.909	35.02 / 0.937
MPRNet [67]	39.31 / 0.972	31.76 / 0.922	35.54 / 0.947
MIMO-UNet+ [12]	- / -	32.05 / 0.921	- / -
MAXIM-3S [60]	39.45 / 0.962	32.84 / 0.935	36.15 / 0.949
BANet [59]	39.55 / 0.971	32.00 / 0.923	35.78 / 0.947
MSSNet [25]	39.76 / 0.972	32.10 / 0.928	35.93 / 0.950
Stripformer [58]	39.84 / 0.974	32.48 / 0.929	36.16 / 0.952
GRL-B [35]	40.20 / 0.974	32.82 / 0.932	36.51 / 0.953
DART-B (ours)	40.23 / 0.975	32.85 / 0.936	36.52 / 0.954

blurring, 4) dual-pixel defocus deblurring and 5) real image denoising, 6) motion deblurring. Details are provided in Tables 3, 4, 5, and 6. In Table 4, we present results for single-image motion deblurring on the real image dataset (GoPro [43]), comparing against the HIDE dataset [51] and in Table 5 the real dataset (RealBlur-R [50]). Across all three datasets, our method, DART-B, surpasses the state-of-the-art [35]. Moving to the analysis of denoising performance on real images in Table 6, our proposed method

Table 6. **Real image denoising** on SIDD [1] and DND [47] datasets. * denotes methods using additional training data. Our is trained only on the SIDD images and directly tested on DND.

Dataset	Method	CBDNet*	RIDNet*	AINDNet*	VDN	SADNet*	DANet+*	CycleISP*	MIRNet	DeamNet*	MPRNet	DAGL	Uformer	Restormer	DART
		[19]	[5]	[26]	[63]	[10]	[64]	[65]	[66]	[49]	[67]	[42]	[62]	[68]	(Ours)
SIDD [1]	PSNR ↑	30.78	38.71	39.08	39.28	39.46	39.47	39.52	39.72	39.47	39.71	38.94	39.77	40.02	40.10
	SSIM ↑	0.801	0.951	0.954	0.956	0.957	0.957	0.957	0.959	0.957	0.958	0.953	0.959	0.960	0.961
DND [47]	PSNR ↑	38.06	39.26	39.37	39.38	39.59	39.58	39.56	39.88	39.63	39.80	39.77	39.96	40.03	40.06
	SSIM ↑	0.942	0.953	0.951	0.952	0.952	0.955	0.956	0.956	0.953	0.954	0.956	0.956	0.956	0.957

Table 7. **SR-DART-B(s) VS DART-B Classical image SR** results. By summarizing the performance on Classical image SR of the network model in the original DART-B, without changing any parameters, we directly reduced the model complexity by two orders of magnitude, and compared the performance with the original Classical image SR’s metrics.

Method	Scale	# Params [M]	Set5 [9]		Set14 [69]		BSD100 [39]		Urban100 [21]		Manga109 [40]	
			PSNR↑	SSIM↑	PSNR↑	SSIM↑	PSNR↑	SSIM↑	PSNR↑	SSIM↑	PSNR↑	SSIM↑
DART-B(s)	×2	17.52	38.66	0.9647	35.06	0.9299	32.69	0.9086	35.07	0.9505	40.65	0.9815
DART-B	×2	25.99	38.69	0.9648	35.11	0.9304	32.72	0.9089	35.10	0.9507	40.71	0.9820
DART-B(s)	×3	14.16	35.01	0.9322	31.00	0.8550	29.50	0.8159	30.18	0.8883	35.40	0.9547
DART-B	×3	20.85	35.10	0.9328	31.05	0.8555	29.55	0.8163	30.22	0.8888	35.46	0.9551
DART-B(s)	×4	14.12	33.03	0.9088	29.32	0.8052	27.98	0.7606	28.51	0.8501	32.78	0.9311
DART-B	×4	20.81	33.12	0.9095	29.39	0.8059	28.02	0.7610	28.55	0.8505	32.81	0.9326

Table 8. **Ablation research** the key design of the attention module on the 2XSR task of the Set5 data set.

LongIR	Feature	Positional	PSNR	SSIM
		✓	38.27	0.9615
✓			38.31	0.9620
✓	✓		38.45	0.9625

outperforms current state-of-the-art techniques.

To further improve the efficiency, we introduce this collaborative image recovery model that integrates multiple attention mechanisms. In another experiment to significantly reduce the model complexity DART-B(s) while maintaining the original DART-B network model, we observed that DART-B(s) has one-third fewer model parameters per SR and a corresponding reduction in training time, but the image restoration results are very close (Table 7). The DART-B(s) and the DART-S(ours) in Table 2 have the network settings and weights are completely different, specifically the experiments of DART-B(s) proved the very strong robustness of our DART network, more details and results are put in the Supplementary Material.

Finally, we conducted a comprehensive ablation study on the Set5 dataset using X2 classical image super-resolution, evaluating the impact of each key component on the proposed model and investigating the effectiveness of three different designs of our proposed model. The results are shown in Table 8. Comparing the LongIR model with the Positional Dimension and Feature Dimension models, we observed improvements of 0.18dB and 0.14dB, respectively, with our DART model. In the LAM (Local Attention Map) experimental study, Figure 7, demonstrate that the proposed DART network exhibits outstanding performance in SR reconstruction by utilizing a wider pixel range.

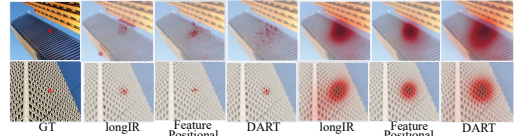


Figure 7. LAM [17] different receptive fields in ablation trials. Darker colors indicate greater contributions, larger red areas indicate that a larger range of contextual information was used. Proposed DART network, compared with each key module of the LongIR, feature Dimension, and Positional Dimension networks in the ablation study, demonstrates superior performance in SR reconstruction based on a significantly wider range of pixels.

5. Conclusion

In this paper, we propose DART, a novel and effective image restoration modeling mechanism, a network that integrates the extraction of long sequences, local, global, specific Feature Dimension, and various Positional Dimension information to enable the model to focus on diverse aspects of complex patterns, thereby enhancing its image recovery capabilities to restore fine details. High-resolution images inherently feature intricate patterns and details that demand precise capture, encompassing both Positional Dimension and Feature Dimension (color) information. In the realm of image restoration, it becomes essential to consider features at multiple scales. The design incorporates various attention mechanisms tailored to focus on different scales, facilitating recovery from both local and global contexts. Addressing noise and artifacts in images, which can impede the recovery process, becomes a key aspect. Leveraging diverse attention mechanisms assists in concentrating on noise-free areas while suppressing attention on noisy regions. Based on these insights, we develop the core design of the multi-attention mechanism DART model for image restoration, and our method achieves competitive performance.

References

- [1] Abdelrahman Abdelhamed, Stephen Lin, and Michael S Brown. A high-quality denoising dataset for smartphone cameras. In *Proceedings of the IEEE conference on computer vision and pattern recognition*, pages 1692–1700, 2018. 8
- [2] Abdelrahman Abdelhamed, Radu Timofte, and Michael S Brown. Ntire 2019 challenge on real image denoising: Methods and results. In *Proceedings of the IEEE/CVF Conference on Computer Vision and Pattern Recognition Workshops*, pages 0–0, 2019. 2
- [3] Abdullah Abuolaim and Michael S Brown. Defocus deblurring using dual-pixel data. In *Computer Vision–ECCV 2020: 16th European Conference, Glasgow, UK, August 23–28, 2020, Proceedings, Part X 16*, pages 111–126. Springer, 2020. 2, 7
- [4] Abdullah Abuolaim, Radu Timofte, and Michael S Brown. Ntire 2021 challenge for defocus deblurring using dual-pixel images: Methods and results. In *Proceedings of the IEEE/CVF Conference on Computer Vision and Pattern Recognition*, pages 578–587, 2021. 2
- [5] Saeed Anwar and Nick Barnes. Real image denoising with feature attention. In *Proceedings of the IEEE/CVF international conference on computer vision*, pages 3155–3164, 2019. 8
- [6] Saeed Anwar and Nick Barnes. Densely residual laplacian super-resolution. *IEEE Transactions on Pattern Analysis and Machine Intelligence*, 44(3):1192–1204, 2020. 2
- [7] Saeed Anwar, Salman Khan, and Nick Barnes. A deep journey into super-resolution: A survey. *ACM Computing Surveys (CSUR)*, 53(3):1–34, 2020. 2
- [8] Iz Beltagy, Matthew E Peters, and Arman Cohan. Longformer: The long-document transformer. *arXiv preprint arXiv:2004.05150*, 2020. 4
- [9] Marco Bevilacqua, Aline Roumy, Christine Guillemot, and Marie Line Alberi-Morel. Low-complexity single-image super-resolution based on nonnegative neighbor embedding. 2012. 6, 8
- [10] Meng Chang, Qi Li, Huajun Feng, and Zhihai Xu. Spatial-adaptive network for single image denoising. In *Computer Vision–ECCV 2020: 16th European Conference, Glasgow, UK, August 23–28, 2020, Proceedings, Part XXX 16*, pages 171–187. Springer, 2020. 8
- [11] Hanting Chen, Yunhe Wang, Tianyu Guo, Chang Xu, Yiping Deng, Zhenhua Liu, Siwei Ma, Chunjing Xu, Chao Xu, and Wen Gao. Pre-trained image processing transformer. In *Proceedings of the IEEE/CVF conference on computer vision and pattern recognition*, pages 12299–12310, 2021. 3, 4, 5, 6, 7
- [12] Sung-Jin Cho, Seo-Won Ji, Jun-Pyo Hong, Seung-Won Jung, and Sung-Jea Ko. Rethinking coarse-to-fine approach in single image deblurring. In *Proceedings of the IEEE/CVF international conference on computer vision*, pages 4641–4650, 2021. 2, 7
- [13] Tao Dai, Jianrui Cai, Yongbing Zhang, Shu-Tao Xia, and Lei Zhang. Second-order attention network for single image super-resolution. In *Proceedings of the IEEE/CVF conference on computer vision and pattern recognition*, pages 11065–11074, 2019. 6
- [14] Akshay Dudhane, Syed Waqas Zamir, Salman Khan, Fahad Shahbaz Khan, and Ming-Hsuan Yang. Burst image restoration and enhancement. In *Proceedings of the IEEE/CVF Conference on Computer Vision and Pattern Recognition*, pages 5759–5768, 2022. 2
- [15] Rich Franzen. Kodak lossless true color image suite. *source: http://r0k.us/graphics/kodak*, 4(2):9, 1999. 5
- [16] Hongyun Gao, Xin Tao, Xiaoyong Shen, and Jiaya Jia. Dynamic scene deblurring with parameter selective sharing and nested skip connections. In *Proceedings of the IEEE/CVF conference on computer vision and pattern recognition*, pages 3848–3856, 2019. 7
- [17] Jinjin Gu and Chao Dong. Interpreting super-resolution networks with local attribution maps. In *Proceedings of the IEEE/CVF Conference on Computer Vision and Pattern Recognition*, pages 9199–9208, 2021. 8
- [18] Shuhang Gu, Yawei Li, Luc Van Gool, and Radu Timofte. Self-guided network for fast image denoising. In *Proceedings of the IEEE/CVF International Conference on Computer Vision*, pages 2511–2520, 2019. 2
- [19] Shi Guo, Zifei Yan, Kai Zhang, Wangmeng Zuo, and Lei Zhang. Toward convolutional blind denoising of real photographs. In *Proceedings of the IEEE/CVF conference on computer vision and pattern recognition*, pages 1712–1722, 2019. 8
- [20] Kaiming He, Jian Sun, and Xiaoou Tang. Single image haze removal using dark channel prior. *IEEE transactions on pattern analysis and machine intelligence*, 33(12):2341–2353, 2010. 2
- [21] Jia-Bin Huang, Abhishek Singh, and Narendra Ahuja. Single image super-resolution from transformed self-exemplars. In *Proceedings of the IEEE conference on computer vision and pattern recognition*, pages 5197–5206, 2015. 5, 6, 8
- [22] Andrey Ignatov and Radu Timofte. Ntire 2019 challenge on image enhancement: Methods and results. In *Proceedings of the IEEE/CVF Conference on Computer Vision and Pattern Recognition Workshops*, pages 0–0, 2019. 2
- [23] Ali Karaali and Claudio Rosito Jung. Edge-based defocus blur estimation with adaptive scale selection. *IEEE Transactions on Image Processing*, 27(3):1126–1137, 2017. 7
- [24] Daisuke Kiku, Yusuke Monno, Masayuki Tanaka, and Masatoshi Okutomi. Beyond color difference: Residual interpolation for color image demosaicking. *IEEE Transactions on Image Processing*, 25(3):1288–1300, 2016. 5
- [25] Kiyeon Kim, Seungyong Lee, and Sunghyun Cho. Mssnet: Multi-scale-stage network for single image deblurring. In *European Conference on Computer Vision*, pages 524–539. Springer, 2022. 7
- [26] Yoonsik Kim, Jae Woong Soh, Gu Yong Park, and Nam Ik Cho. Transfer learning from synthetic to real-noise denoising with adaptive instance normalization. In *Proceedings of the IEEE/CVF conference on computer vision and pattern recognition*, pages 3482–3492, 2020. 8
- [27] Johannes Kopf, Boris Neubert, Billy Chen, Michael Cohen, Daniel Cohen-Or, Oliver Deussen, Matt Uyttendaele,

- and Dani Lischinski. Deep photo: Model-based photograph enhancement and viewing. *ACM transactions on graphics (TOG)*, 27(5):1–10, 2008. [2](#)
- [28] Orest Kupyn, Volodymyr Budzan, Mykola Mykhailych, Dmytro Mishkin, and Jiří Matas. Deblurgan: Blind motion deblurring using conditional adversarial networks. In *Proceedings of the IEEE conference on computer vision and pattern recognition*, pages 8183–8192, 2018. [7](#)
- [29] Orest Kupyn, Tetiana Martyniuk, Junru Wu, and Zhangyang Wang. Deblurgan-v2: Deblurring (orders-of-magnitude) faster and better. In *Proceedings of the IEEE/CVF international conference on computer vision*, pages 8878–8887, 2019. [2](#), [7](#)
- [30] Junyong Lee, Sungkil Lee, Sunghyun Cho, and Seungyong Lee. Deep defocus map estimation using domain adaptation. In *Proceedings of the IEEE/CVF conference on computer vision and pattern recognition*, pages 12222–12230, 2019. [7](#)
- [31] Junyong Lee, Hyeonseok Son, Jaesung Rim, Sunghyun Cho, and Seungyong Lee. Iterative filter adaptive network for single image defocus deblurring. In *Proceedings of the IEEE/CVF Conference on Computer Vision and Pattern Recognition*, pages 2034–2042, 2021. [7](#)
- [32] Siyuan Li, Iago Breno Araujo, Wenqi Ren, Zhangyang Wang, Eric K Tokuda, Roberto Hirata Junior, Roberto Cesar Junior, Jiawan Zhang, Xiaojie Guo, and Xiaochun Cao. Single image deraining: A comprehensive benchmark analysis. In *Proceedings of the IEEE/CVF Conference on Computer Vision and Pattern Recognition*, pages 3838–3847, 2019. [2](#)
- [33] Wenbo Li, Xin Lu, Shengju Qian, Jiangbo Lu, Xiangyu Zhang, and Jiaya Jia. On efficient transformer-based image pre-training for low-level vision. *arXiv preprint arXiv:2112.10175*, 2021. [5](#), [6](#)
- [34] Xia Li, Jianlong Wu, Zhouchen Lin, Hong Liu, and Hongbin Zha. Recurrent squeeze-and-excitation context aggregation net for single image deraining. In *Proceedings of the European conference on computer vision (ECCV)*, pages 254–269, 2018. [2](#)
- [35] Yawei Li, Yuchen Fan, Xiaoyu Xiang, Denis Demandolx, Rakesh Ranjan, Radu Timofte, and Luc Van Gool. Efficient and explicit modelling of image hierarchies for image restoration. In *Proceedings of the IEEE/CVF Conference on Computer Vision and Pattern Recognition*, pages 18278–18289, 2023. [1](#), [2](#), [5](#), [6](#), [7](#)
- [36] Jingyun Liang, Jiezhong Cao, Guolei Sun, Kai Zhang, Luc Van Gool, and Radu Timofte. Swinir: Image restoration using swin transformer. In *Proceedings of the IEEE/CVF international conference on computer vision*, pages 1833–1844, 2021. [1](#), [2](#), [3](#), [5](#), [6](#)
- [37] Xing Liu, Masanori Suganuma, Zhun Sun, and Takayuki Okatani. Dual residual networks leveraging the potential of paired operations for image restoration. In *Proceedings of the IEEE/CVF Conference on Computer Vision and Pattern Recognition*, pages 7007–7016, 2019. [2](#)
- [38] Ze Liu, Yutong Lin, Yue Cao, Han Hu, Yixuan Wei, Zheng Zhang, Stephen Lin, and Baining Guo. Swin transformer: Hierarchical vision transformer using shifted windows. In *Proceedings of the IEEE/CVF international conference on computer vision*, pages 10012–10022, 2021. [1](#), [3](#), [4](#)
- [39] David Martin, Charless Fowlkes, Doron Tal, and Jitendra Malik. A database of human segmented natural images and its application to evaluating segmentation algorithms and measuring ecological statistics. In *Proceedings Eighth IEEE International Conference on Computer Vision. ICCV 2001*, pages 416–423. IEEE, 2001. [5](#), [6](#), [8](#)
- [40] Yusuke Matsui, Kota Ito, Yuji Aramaki, Azuma Fujimoto, Toru Ogawa, Toshihiko Yamasaki, and Kiyoharu Aizawa. Sketch-based manga retrieval using manga109 dataset. *Multimedia Tools and Applications*, 76:21811–21838, 2017. [6](#), [8](#)
- [41] Tomer Michaeli and Michal Irani. Nonparametric blind super-resolution. In *Proceedings of the IEEE International Conference on Computer Vision*, pages 945–952, 2013. [2](#)
- [42] Chong Mou, Jian Zhang, and Zhuoyuan Wu. Dynamic attentive graph learning for image restoration. In *Proceedings of the IEEE/CVF international conference on computer vision*, pages 4328–4337, 2021. [8](#)
- [43] Seungjun Nah, Tae Hyun Kim, and Kyoung Mu Lee. Deep multi-scale convolutional neural network for dynamic scene deblurring. In *Proceedings of the IEEE conference on computer vision and pattern recognition*, pages 3883–3891, 2017. [7](#)
- [44] Seungjun Nah, Sanghyun Son, Suyoung Lee, Radu Timofte, and Kyoung Mu Lee. Ntire 2021 challenge on image deblurring. In *Proceedings of the IEEE/CVF Conference on Computer Vision and Pattern Recognition*, pages 149–165, 2021. [2](#)
- [45] Ben Niu, Weilei Wen, Wenqi Ren, Xiangde Zhang, Lianping Yang, Shuzhen Wang, Kaihao Zhang, Xiaochun Cao, and Haifeng Shen. Single image super-resolution via a holistic attention network. In *Computer Vision—ECCV 2020: 16th European Conference, Glasgow, UK, August 23–28, 2020, Proceedings, Part XII 16*, pages 191–207. Springer, 2020. [6](#)
- [46] Dongwon Park, Dong Un Kang, Jisoo Kim, and Se Young Chun. Multi-temporal recurrent neural networks for progressive non-uniform single image deblurring with incremental temporal training. In *European Conference on Computer Vision*, pages 327–343. Springer, 2020. [7](#)
- [47] Tobias Plotz and Stefan Roth. Benchmarking denoising algorithms with real photographs. In *Proceedings of the IEEE conference on computer vision and pattern recognition*, pages 1586–1595, 2017. [8](#)
- [48] Kuldeep Purohit, Maitreya Suin, AN Rajagopalan, and Vishnu Naresh Boddeti. Spatially-adaptive image restoration using distortion-guided networks. In *Proceedings of the IEEE/CVF International Conference on Computer Vision*, pages 2309–2319, 2021. [7](#)
- [49] Chao Ren, Xiaohai He, Chuncheng Wang, and Zhibo Zhao. Adaptive consistency prior based deep network for image denoising. In *Proceedings of the IEEE/CVF conference on computer vision and pattern recognition*, pages 8596–8606, 2021. [8](#)
- [50] Jaesung Rim, Haeyun Lee, Jucheol Won, and Sunghyun Cho. Real-world blur dataset for learning and benchmarking deblurring algorithms. In *Computer Vision—ECCV 2020: 16th European Conference, Glasgow, UK, August 23–28, 2020*,

- Proceedings, Part XXV 16*, pages 184–201. Springer, 2020. 7
- [51] Ziyi Shen, Wenguan Wang, Xiankai Lu, Jianbing Shen, Haibin Ling, Tingfa Xu, and Ling Shao. Human-aware motion deblurring. In *Proceedings of the IEEE/CVF International Conference on Computer Vision*, pages 5572–5581, 2019. 7
- [52] Jianping Shi, Li Xu, and Jiaya Jia. Just noticeable defocus blur detection and estimation. In *Proceedings of the IEEE Conference on Computer Vision and Pattern Recognition*, pages 657–665, 2015. 7
- [53] Hyeonseok Son, Junyong Lee, Sunghyun Cho, and Seungyong Lee. Single image defocus deblurring using kernel-sharing parallel atrous convolutions. In *Proceedings of the IEEE/CVF International Conference on Computer Vision*, pages 2642–2650, 2021. 7
- [54] Maitreya Suin, Kuldeep Purohit, and AN Rajagopalan. Spatially-attentive patch-hierarchical network for adaptive motion deblurring. In *Proceedings of the IEEE/CVF conference on computer vision and pattern recognition*, pages 3606–3615, 2020. 7
- [55] Xin Tao, Hongyun Gao, Xiaoyong Shen, Jue Wang, and Jiaya Jia. Scale-recurrent network for deep image deblurring. In *Proceedings of the IEEE conference on computer vision and pattern recognition*, pages 8174–8182, 2018. 7
- [56] Chunwei Tian, Lunke Fei, Wenxian Zheng, Yong Xu, Wangmeng Zuo, and Chia-Wen Lin. Deep learning on image denoising: An overview. *Neural Networks*, 131:251–275, 2020. 2
- [57] Radu Timofte, Vincent De Smet, and Luc Van Gool. Anchored neighborhood regression for fast example-based super-resolution. In *Proceedings of the IEEE international conference on computer vision*, pages 1920–1927, 2013. 2
- [58] Fu-Jen Tsai, Yan-Tsung Peng, Yen-Yu Lin, Chung-Chi Tsai, and Chia-Wen Lin. Stripformer: Strip transformer for fast image deblurring. In *European Conference on Computer Vision*, pages 146–162. Springer, 2022. 7
- [59] Fu-Jen Tsai, Yan-Tsung Peng, Chung-Chi Tsai, Yen-Yu Lin, and Chia-Wen Lin. Banet: a blur-aware attention network for dynamic scene deblurring. *IEEE Transactions on Image Processing*, 31:6789–6799, 2022. 7
- [60] Zhengzhong Tu, Hossein Talebi, Han Zhang, Feng Yang, Peyman Milanfar, Alan Bovik, and Yinxiao Li. Maxim: Multi-axis mlp for image processing. In *Proceedings of the IEEE/CVF Conference on Computer Vision and Pattern Recognition*, pages 5769–5780, 2022. 7
- [61] Ashish Vaswani, Noam Shazeer, Niki Parmar, Jakob Uszkoreit, Llion Jones, Aidan N Gomez, Łukasz Kaiser, and Illia Polosukhin. Attention is all you need. *Advances in neural information processing systems*, 30, 2017. 1
- [62] Zhendong Wang, Xiaodong Cun, Jianmin Bao, Wengang Zhou, Jianzhuang Liu, and Houqiang Li. Uformer: A general u-shaped transformer for image restoration. In *Proceedings of the IEEE/CVF conference on computer vision and pattern recognition*, pages 17683–17693, 2022. 2, 7, 8
- [63] Zongsheng Yue, Hongwei Yong, Qian Zhao, Deyu Meng, and Lei Zhang. Variational denoising network: Toward blind noise modeling and removal. *Advances in neural information processing systems*, 32, 2019. 8
- [64] Zongsheng Yue, Qian Zhao, Lei Zhang, and Deyu Meng. Dual adversarial network: Toward real-world noise removal and noise generation. In *Computer Vision–ECCV 2020: 16th European Conference, Glasgow, UK, August 23–28, 2020, Proceedings, Part X 16*, pages 41–58. Springer, 2020. 2, 8
- [65] Syed Waqas Zamir, Aditya Arora, Salman Khan, Munawar Hayat, Fahad Shahbaz Khan, Ming-Hsuan Yang, and Ling Shao. Cycleisp: Real image restoration via improved data synthesis. In *Proceedings of the IEEE/CVF conference on computer vision and pattern recognition*, pages 2696–2705, 2020. 8
- [66] Syed Waqas Zamir, Aditya Arora, Salman Khan, Munawar Hayat, Fahad Shahbaz Khan, Ming-Hsuan Yang, and Ling Shao. Learning enriched features for real image restoration and enhancement. In *Computer Vision–ECCV 2020: 16th European Conference, Glasgow, UK, August 23–28, 2020, Proceedings, Part XXV 16*, pages 492–511. Springer, 2020. 2, 8
- [67] Syed Waqas Zamir, Aditya Arora, Salman Khan, Munawar Hayat, Fahad Shahbaz Khan, Ming-Hsuan Yang, and Ling Shao. Multi-stage progressive image restoration. In *Proceedings of the IEEE/CVF conference on computer vision and pattern recognition*, pages 14821–14831, 2021. 2, 7, 8
- [68] Syed Waqas Zamir, Aditya Arora, Salman Khan, Munawar Hayat, Fahad Shahbaz Khan, and Ming-Hsuan Yang. Restormer: Efficient transformer for high-resolution image restoration. In *Proceedings of the IEEE/CVF conference on computer vision and pattern recognition*, pages 5728–5739, 2022. 1, 2, 3, 5, 7, 8
- [69] Roman Zeyde, Michael Elad, and Matan Protter. On single image scale-up using sparse-representations. In *Curves and Surfaces: 7th International Conference, Avignon, France, June 24-30, 2010, Revised Selected Papers 7*, pages 711–730. Springer, 2012. 6, 8
- [70] Hongguang Zhang, Yuchao Dai, Hongdong Li, and Piotr Koniusz. Deep stacked hierarchical multi-patch network for image deblurring. In *Proceedings of the IEEE/CVF Conference on Computer Vision and Pattern Recognition*, pages 5978–5986, 2019. 7
- [71] Kai Zhang, Wangmeng Zuo, Yunjin Chen, Deyu Meng, and Lei Zhang. Beyond a gaussian denoiser: Residual learning of deep cnn for image denoising. *IEEE transactions on image processing*, 26(7):3142–3155, 2017. 5
- [72] Kaihao Zhang, Wenhan Luo, Yiran Zhong, Lin Ma, Bjorn Stenger, Wei Liu, and Hongdong Li. Deblurring by realistic blurring. In *Proceedings of the IEEE/CVF Conference on Computer Vision and Pattern Recognition*, pages 2737–2746, 2020. 7
- [73] Kai Zhang, Yawei Li, Wangmeng Zuo, Lei Zhang, Luc Van Gool, and Radu Timofte. Plug-and-play image restoration with deep denoiser prior. *IEEE Transactions on Pattern Analysis and Machine Intelligence*, 44(10):6360–6376, 2021. 2, 5
- [74] Lei Zhang, Xiaolin Wu, Antoni Buades, and Xin Li. Color demosaicking by local directional interpolation and nonlocal

adaptive thresholding. *Journal of Electronic imaging*, 20(2): 023016–023016, 2011. [5](#)

- [75] Yulun Zhang, Kunpeng Li, Kai Li, Lichen Wang, Bineng Zhong, and Yun Fu. Image super-resolution using very deep residual channel attention networks. In *Proceedings of the European conference on computer vision (ECCV)*, pages 286–301, 2018. [2](#), [6](#)
- [76] Yulun Zhang, Kunpeng Li, Kai Li, Bineng Zhong, and Yun Fu. Residual non-local attention networks for image restoration. *arXiv preprint arXiv:1903.10082*, 2019. [2](#), [5](#)
- [77] Yulun Zhang, Yapeng Tian, Yu Kong, Bineng Zhong, and Yun Fu. Residual dense network for image restoration. *IEEE transactions on pattern analysis and machine intelligence*, 43(7):2480–2495, 2020. [2](#)